

Pronounced effects of additional resistance in Andreev reflection spectroscopyT. Y. Chen,^{*} S. X. Huang, and C. L. Chien*Department of Physics and Astronomy, The Johns Hopkins University, Baltimore, Maryland 21218, USA*

(Received 2 September 2009; revised manuscript received 8 November 2009; published 28 June 2010)

We present a systematic investigation of the additional resistance (R_E), which is an unavoidable consequence of pseudo-four-probe electrical measurements, on the point-contact Andreev reflection (PCAR) spectrum by both modeling and experiments. Instead of considering the total resistance between the two voltage leads across a point contact as a sum of a contact resistance (R_C) and a fixed sample resistance (R_S), it is essential to treat the total resistance as a sum of the Andreev resistance R_{AR} and the additional resistance R_E , which are, respectively, the resistances affected and unaffected by the Andreev reflection process. We show a detailed formalism of taking R_E into account in modeling and demonstrate that the PCAR spectrum can be drastically affected by the presence of R_E . Experimentally, we have found that not only R_E cannot be readily measured or even estimated, it is in fact different for each contact, depending on the contact resistance and whether the contact is near the purely ballistic regime or the purely diffusive regime. A self-consistent process is necessary to analyze the entire PCAR spectrum, properly normalize the conductance, determine R_E , and other parameters including the spin polarization and the superconducting gap for each contact. We determine R_E for various contacts on specimens with different resistivity and resolve the causes of R_E . For contacts close to the diffusive regime, there are two sources of R_E : a dominant contribution which is linearly proportional to the total resistance and a constant value from the sample resistance. We also address the effects of additional resistance when PCAR is administered in the ballistic limit and in the diffusive limit. With the proper treatment of the additional resistance, we demonstrate that PCAR can quantitatively extract essential information of spin polarization and superconducting gap.

DOI: [10.1103/PhysRevB.81.214444](https://doi.org/10.1103/PhysRevB.81.214444)

PACS number(s): 74.45.+c, 74.50.+r, 74.25.F-, 72.25.Mk

I. INTRODUCTION

The performance of many spin devices, such as giant magnetoresistance field sensors and magnetic tunnel junctions, is greatly enhanced if highly spin-polarized materials are used. The search for materials with high spin polarization (P), especially half metals with $P=100\%$, has been a major subject in spin electronics.^{1,2}

The spin polarization is defined as $P=(n_{\uparrow}-n_{\downarrow})/(n_{\uparrow}+n_{\downarrow})$, the imbalance of density of spin-up (n_{\uparrow}) and spin-down (n_{\downarrow}) electrons at the Fermi energy. Despite its importance, only a few techniques can measure the value of P of a ferromagnet (F), each with inherent advantages and shortcomings. The spin-dependent tunneling method,³ notably the F/insulator/superconductor (F/I/S) and $F_1/I/F_2$ tunnel junctions, measures the spin density of states of a F via either the density of states of the S as in F/I/S junctions or that of another ferromagnet as in $F_1/I/F_2$ tunnel junctions, across a thin I barrier. The characteristics of such tunnel junctions, and consequently the determined value of P , depend sensitively on the quality and the characteristics of the tunnel barrier of only about 1 nm in thickness. For instance, the P value of Fe as deduced from the $F_1/I/F_2$ tunnel junctions varies greatly according to the tunnel resistance value, which depends sensitively on the quality of the Al_2O_3 tunnel barrier.^{4,5} In MgO tunnel junctions, because of the unique coherent tunneling process in crystalline (001) MgO, the deduced value of P is altogether different.⁶ Even the sign of P of ferromagnetic Co can be different between junctions using Al_2O_3 and $SrTiO_3$.⁷ Spin-resolved photoemission is another method that can measure the spin polarization of photoelectrons emitted from the surface of a ferromagnet using Mott scattering.⁸ How-

ever, photoemission is highly susceptible to surface contamination and surface states. In some cases, notably Ni, widely different values of P from 15% to 100% have been reported by such measurements.^{9,10}

II. POINT-CONTACT ANDREEV REFLECTION SPECTROSCOPY

Point-contact Andreev reflection (PCAR) spectroscopy is another method that utilizes the density of states of a superconductor to measure the value of P of a material of interest. At the interface of an S and a normal metal (N), an incident electron with energy within the superconducting gap (2Δ) must be accompanied by another electron of the opposite spin to enter the superconductor as a Cooper pair. This is equivalent to reflecting a hole back to the normal metal, thus doubling the conductance. This is the well-known Andreev reflection (AR) process¹¹ in which a normal current is converted into a supercurrent. In a spin-polarized current from a ferromagnet, the depletion of electrons with one spin direction suppresses the AR process, thus leading to the PCAR spectroscopy, which is a more recent technique that can quantitatively determine the P value of a ferromagnet as well as the value of the superconducting gap.¹²

Since the first experimental demonstration,^{13,14} the PCAR technique has been greatly improved, especially in the quantitative data analysis, to extract the P value. Initially, clean contacts were assumed and the conductance ratio $G(0)/G_n = 2(1-P)$ between the conductance at zero-bias voltage ($V=0$) within the superconducting gap and the conductance in the normal state was used to extract P .¹⁴ It was soon realized that real contacts were rarely ideal and the entire conduc-

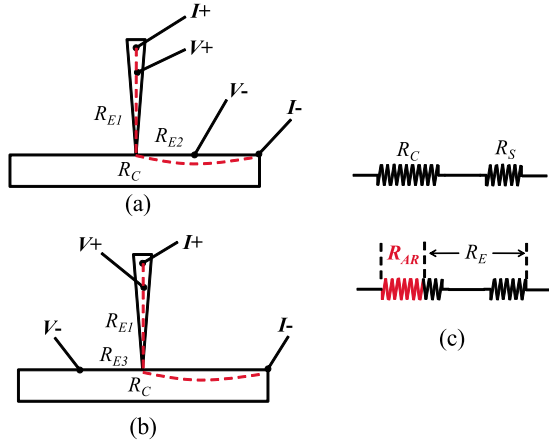


FIG. 1. (Color online) Schematics of two typical point-contact experiments with possible causes of extra resistance indicated as R_{E1} and R_{E2} in (a) and R_{E1} and R_{E3} in (b) and with current path indicated as dashed line. (c) Schematics of the Andreev resistance R_{AR} , contact resistance R_C , sample resistance R_S , and extra resistance R_E .

tance curve, with the inclusion of interfacial scattering factor Z and thermal smearing due to finite temperature, should be analyzed to determine the P value.^{15–17} Later on, AR process in the diffusive regime has been addressed,¹⁸ three-dimensional effect and inelastic scattering¹⁹ have also been incorporated into the model to extract P quantitatively. The P values of many ferromagnets^{13,14,17–26} have since been determined by the PCAR technique, including some highly spin-polarized materials^{22–24} and even half metals^{25,26} in which only one spin band is available at the Fermi level.

III. ADDITIONAL RESISTANCE IN PCAR SPECTROSCOPY

In Andreev reflection spectroscopy, only the electrical resistance at the point contact (R_C) contains the relevant information of the Andreev reflection, the superconducting gap and the spin polarization. However, in actual PCAR measurements, the electrical contacts were made close to, but not at, the point contact in the pseudo-four-probe arrangements as shown in Figs. 1(a) and 1(b). As schematically shown by the current paths in Fig. 1, the measured resistance by the pseudo-four-probe methods also includes extra resistance called the spreading resistance or the sample resistance (R_S).^{27,28} When bulk samples with low resistivity are used, the contribution of R_S is so small that the measured resistance is essentially just R_C .

On the other hand, when material with a larger resistivity and especially when thin films are involved, not only R_S is not negligible, it can even be larger than R_C . The effects of a significant R_S are often disguised as a larger than expected superconducting gap²⁶ and an effective temperature higher than the actual temperature of the measurement in order to satisfactorily fit the PCAR spectra.^{28,29} However, such a practice may compromise the confidence in the determined values of the spin polarization or the superconducting gap. One may attempt to minimize R_S by placing the voltage elec-

trode as close to the point contact as possible or attempt to measure R_S by systematically varying the location of the voltage lead. One may also incorporate sample resistance R_S as an additional fitting parameter as has indeed been previously suggested.^{27,28} However, with R_S so included, the experimental conductance can no longer be correctly normalized and thus *cannot* be compared directly with the theoretical models. Therefore great care must be taken when including R_S into the model and the cause of R_S must be addressed. As shown by this work, these measures fall far short of addressing the pronounced effects of the additional resistance problem in PCAR spectroscopy, in particular, and point-contact electrical measurements in general.

In this work, we describe a systematic investigation of the additional resistance in the PCAR spectroscopy using both modeling and experiments. We show that the additional resistance originates not only from the sample resistance as one suspects but also from the contact itself. The variation in additional resistance with the location of the contact is highly nonlinear, thus cannot be alleviated by strategically placing the electrodes close to the main point contact. Nor can the additional resistance be measured even if one does not alter the measuring geometry. Previously, it has been suggested that an additional sample resistance R_S be added to the contact resistance R_C .^{27,28} Furthermore, the value of R_S is fixed since it originates from region away from the contact. As shown in this work, it is imperative to separate the total measured resistance as

$$R = R_{AR} + R_E, \quad (1)$$

which is a sum of the Andreev resistance R_{AR} from the contact region where AR process occurs and the additional resistance R_E which is *not* affected by the AR process. The value of R_E have contributions from both the region away from the contact *and* from the contact region [Fig. 1(c)]. Consequently, the value of R_E is not fixed but varies from contact to contact. We show that the PCAR spectra are not only drastically affected by the presence of R_E , more importantly, the separation of R_{AR} and R_E enables one to correctly address the crucial normalization issue, which otherwise cannot be correctly performed had one assumed $R = R_C + R_S$. Experimentally, we find that R_E cannot be reliably measured or even estimated because it is different for each contact depending on the contact resistance and whether the contact is near the purely ballistic limit or the purely diffusive limit. A self-consistent process is therefore necessary to analyze the entire PCAR spectrum to determine R_E and other parameters including the spin polarization and the superconducting gap for each contact. We determine R_E , R_{AR} , R_S , and R_C for various contacts on specimens with different resistivity and resolve the causes of R_E . For contacts on high-resistivity samples close to the diffusive limit, R_E has two sources: a small and constant term due to the sample resistance, and a dominant contribution, which is linearly proportional to the total resistance. For contacts on specimens with a modest resistivity R_E also follows a systematic trend on the total resistance.

IV. SOURCES OF ADDITIONAL RESISTANCE

In the point-contact geometry, the two voltage electrodes not only measure the contact resistance R_C but also additional resistances from the tip through the sample along the current path, for example, $R_C+R_{E1}+R_{E2}$ in Fig. 1(a) and $R_C+R_{E1}+R_{E3}$ in Fig. 1(b). In PCAR experiments using a superconducting tip, R_{E1} may be negligible but not R_{E2} or R_{E3} . Between the two configurations in Figs. 1(a) and 1(b), one might prefer the one in Fig. 1(b) since R_{E3} might be different from, and perhaps much less than, R_{E2} . However, as described below, the contribution to the additional resistance in PCAR stems from the fact that the AR process occurs only near the contact interface. Any resistance in the current path not affected by the AR process contributes to the additional resistance, which cannot be eliminated by manipulating the electrodes.

Since PCAR on a thin film is one common situation where the large sample resistance contributes significantly to the additional resistance, we first discuss the current distribution in the plane of a thin-film sample. Consider two current contacts A of radius a and B of radius b ($b \gg a$) at a distance d away on a thin film of thickness t with a current I_o flowing from A to B . For simplicity, we assume the film to be very thin and focus on the distribution of the current in the film plane, neglecting variation within the film thickness. This problem becomes effectively a two-dimensional electrostatic problem and the potential $\varphi(x, y)$ in the thin-film plane can be solved analytically using the image method with the results of

$$\varphi(x, y) = \frac{I_o \rho}{4 \pi t} \ln \frac{(x+c)^2 + y^2}{(x-c)^2 + y^2},$$

$$c = \sqrt{\frac{(d^2 - a^2 - b^2)^2 - 4a^2b^2}{4d^2}}, \quad (2)$$

taking the midpoint between the two images as the origin, where ρ is the resistivity of the thin film. The sheet resistance between the point contact A and a voltage lead located at any point in the film plane can be calculated from this potential. In particular, the sheet resistance ρ/t between point A and any point along the line on which A and B lie is shown in Fig. 2(b), using the contact sizes $a=30$ nm and $b=127$ μm and the distance $d=2$ mm, which are typical values used in our experiments. First of all, the sheet resistance increases with distance from A in a highly nonlinear manner, increasing especially rapidly in the immediate vicinity of contact A . At a distance of only $700a=21$ μm from the contact A , the sheet resistance has already reached half of the value at $d=2$ mm. These results indicate that it is fruitless to attempt to place the voltage electrode close to the point contact to alleviate the additional resistance since much of the resistance has been acquired within the proximity of the point contact A . The results also demonstrate that thin film far from the contact ($\gg 10a$) still contributes significantly to the overall resistance. The calculations also address the merit of the two experimental situations shown in Figs. 1(a) and 1(b), which correspond to point C and D , respectively, in Figs. 2(a) and 2(b). The resistance at D is indeed lower than

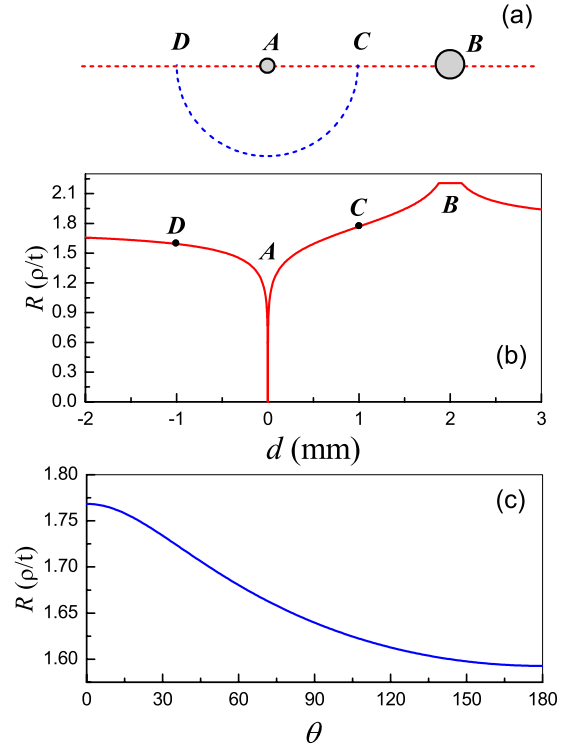


FIG. 2. (Color online) Calculated sheet resistance on a thin film with resistivity ρ and thickness t between a voltage lead and the point contact A . (a) Schematics of a point contact and a current lead with radius of 30 nm and 127 μm and a separation of 2 mm on a thin-film plane, (b) resistance between A and a voltage lead along the dashed line in (a), and (c) resistance between A and voltage lead on the half circle from C to D in (a).

that at C but only slightly by about 10% due to the dominant contribution to the total resistance in the vicinity of the point contact. We have calculated the resistance on a semicircle from C to D and found the resistance to decrease monotonically by about 10% as shown in Fig. 2(c). With a voltage contact at D , the additional resistance in the scheme in Fig. 1(b) is definitely not negligible.

V. ADDITIONAL RESISTANCE IN THE DIFFUSIVE AND BALLISTIC LIMITS

When a diffusive point contact is formed, the contact resistance is $[\rho/\pi a]\tan^{-1}(x/a)$,³⁰ where x is the distance from the center of the contact. The Maxwell form of total resistance of $\rho/2a$ is reached by letting $x \rightarrow \infty$. However, at $x=a$, the resistance is only half of the Maxwell resistance illustrating that other parts far from the contact also contributes substantially.

In the cases discussed above, the measured resistance includes the resistance at the contact region as well as those of other parts away from the contact. In a PCAR experiment, the contact resistance is the resistance of the contact region. However, only a portion of the contact resistance undergoes the AR process as denoted by R_{AR} . The rest of the measured resistance includes resistance away from the contact as well as a portion of the contact resistance unaffected by the AR

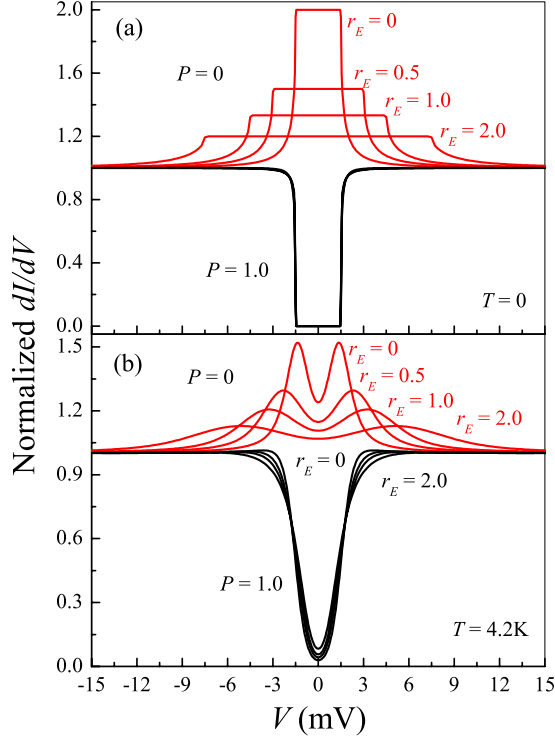


FIG. 3. (Color online) Calculated PCAR spectra in the purely ballistic regime with various $r_E=0,0.5,1.0,2.0$ for $P=0$ and 1.0 at (a) $T=0$ and (b) $T=4.2$ K.

process. Therefore the total resistance between the point contact and the voltage electrode in a PCAR experiment is, as described in Eq. (1), $R=R_{AR}+R_E$ [Fig. 1(c) bottom], a sum of resistances affected and unaffected by the AR process. This definition, which differs fundamentally from previous work^{27,28} where the total resistance $R=R_C+R_S$ [Fig. 1(c) top] is defined as the sum of the contact resistance R_C and a fixed sample resistance R_S is crucial for the understanding of the experimental situation as described below.

The above discussion is for diffusive point contacts. For a purely ballistic point contact, the contact resistance is the Sharvin resistance of $4\rho l/3\pi a^2$, which is due to the constraint of the aperture of radius a .³¹ Current far from the contact is still diffusive thus there should also be some additional resistance. But in this case the additional resistance is at most the Maxwell resistance $\rho/2a$, and in the ballistic limit ($l \gg a$), $\rho/2a \ll 4\rho l/3\pi a^2$, thus it is negligible. However, in an actual experiment, a point contact is neither purely ballistic nor purely diffusive, the extra resistance R_E is therefore unavoidable. Our discussion indicates that a portion of the contact resistance, which is not affected by the AR process, contributes to the additional resistance R_E . This means that R_E cannot be experimentally measured without knowing the region where the AR process applies. Next, we describe the formalism that includes R_E and discuss its effects on the PCAR spectra and then demonstrate the methods for determining R_{AR} , R_E , R_C , and R_S experimentally in PCAR experiments.

VI. NORMALIZATION OF DIFFERENTIAL CONDUCTANCE

The differential conductance of a N/S point contact with a bias voltage V_{AR} can be calculated from the current I_{NS} ,³²

$$\frac{dI_{NS}}{dV_{AR}} = 2eS_C N v_F \int_{-\infty}^{\infty} \left[\frac{df(E - eV_{AR}, T)}{dV_{AR}} \right] [1 + A - B] dE, \quad (3)$$

where f is the Fermi distribution function, e the electron charge, S_C the effective contact area, N the spin density of states, v_F the Fermi velocity, A the AR probability, B the normal reflection probability, and V_{AR} the voltage on the region where the AR process occurs. At very large voltages ($V_{AR} \gg \Delta$), the superconductor at the interface becomes normal and without the AR process thus $A=0$ and $B=1/(Z^2+1)$. The differential conductance can be integrated analytically with $dI_{NN}/dV_{AR}=2Ne^2S_C v_F/(1+Z^2) \equiv 1/R_{NN}$ as the normalization conductance for dI_{NS}/dV_{AR} . The normalization conductance $1/R_{NN}$ is of crucial importance allowing us to avoid knowing the detailed values of the parameters of N , S_C , and v_F of the point contact. However, one can experimentally only measure dI_{NS}/dV but not dI_{NS}/dV_{AR} . Furthermore, dI_{NS}/dV cannot be normalized by $1/R_{NN}$ because of the additional resistance R_E , where V is the total voltage including the voltage V_{AR} and the voltage V_E from the extra resistance. The actual measured differential conductance is

$$\begin{aligned} \frac{dI_{NS}}{dV} &= \frac{\Delta I_{NS}}{\Delta V} = \frac{\Delta I_{NS}}{\Delta V_{AR} + \Delta I_{NS} R_E} \\ &= \frac{R_{NN} \frac{dI_{NS}}{dV_{AR}}}{R_{NN} + R_{NN} R_E \frac{dI_{NS}}{dV_{AR}}} \\ &= \frac{1}{R_{NN} \left(1 + r_E \left(\frac{dI_{NS}}{dV_{AR}} \right)_0 \right)} \end{aligned} \quad (4)$$

with $(dI_{NS}/dV_{AR})_0 = R_{NN}(dI_{NS}/dV_{AR})$ as the normalized conductance and $r_E \equiv R_E/R_{NN}$ as the relative additional resistance. At large bias voltage ($V \gg \Delta$), $(dI_{NS}/dV_{AR})_0 = 1$. So the normalization resistance for dI_{NS}/dV is $R_{NN}(1+r_E)$. We now have

$$\begin{aligned} (dI_{NS}/dV)_0 &= R_{NN}(1+r_E) dI_{NS}/dV \\ &= (1+r_E)(dI_{NS}/dV_{AR})_0 [1+r_E(dI_{NS}/dV_{AR})_0]. \end{aligned} \quad (5)$$

This formula is independent of R_{NN} , which depends on detailed value of S_C , v_F , and N of the contact. More importantly, it should be noted that the normalization of dI_{NS}/dV by $R_{NN}(1+r_E)$ allows the correct normalization of dI_{NS}/dV_{AR} .

VII. EFFECTS OF ADDITIONAL RESISTANCE ON PCAR SPECTRUM

Equation (5) together with $V = V_{AR} + R_E I_{NS}$ can be used to calculate the PCAR spectrum dI_{NS}/dV as a function of V using V_{AR} as a parameter. Figure 3(a) shows some of the calculated PCAR spectra with different r_E of 0.0, 0.5, 1, and 2 for spin polarization $P=0$ and $P=1$ using the ballistic model at temperature $T=0$. In the case of an unpolarized metal of $P=0$, there are very substantial effects of the additional resistance which reduces and broadens the two AR peaks. For example, the normalized conductance is 2 for $r_E=0$ as expected but reduces to only 1.33 for $r_E=1$. This is because the AR process occurs only at the contact interface and affects only the contact resistance R_{AR} but not R_E . Consequently, only R_{AR} becomes $R_{NN}/2$ for $V_{AR} \leq \Delta$ while R_E remains the same. Therefore the conductance is $2R_{NN}/(R_{NN}/2 + R_{NN}) = 1.33$ for $r_E=1$.

On the other hand, the value of $r_E=0$ to $r_E=2$ has no effects on the PCAR spectra for $P=1$ at $T=0$ as shown in Fig. 3(a). This is because the contact resistance R_{AR} is infinite ($\gg R_E$) due to the complete suppression of the AR process by the half metallicity, consequently a negligible dependence on R_E . In Fig. 3(b) we show some calculated PCAR spectra at $T=4.2$ K with the interfacial scattering factor $Z=0.5$. The additional resistance again suppresses and broadens the PCAR spectra. Interestingly, contrary to that of the half-metallic case with $P=1$ and at $T=0$, r_E has a noticeable effect on the spectra even for $P=1$ at 4.2 K, as shown in Fig. 3(b). This is because at finite temperatures, R_{AR} at $|V| < \Delta/e$ is also finite thus some voltage on the additional resistance R_E , causing the observable difference.

A very important consequence of the finite additional resistance R_E is that the apparent superconducting gap increases significantly as mentioned earlier. The two AR peaks are often used to mark the superconducting gap. As shown in Fig. 3(b), the two AR peaks correctly appear at $\pm\Delta/e$ when $r_E \approx 0$. However, when r_E is significant, the two apparent AR peaks shifts to values larger than $\pm\Delta/e$. At $r_E=0.5, 1.0$, and 2.0 , the apparent gap becomes $2\Delta/e, 3\Delta/e$, and $5\Delta/e$, respectively. In fact, the apparent superconducting gap varies as $(1+2r_E)\Delta$, a very noticeable effect at a significant r_E , leading one to conclude erroneously a larger superconducting gap.

Some PCAR spectra have been calculated using the purely diffusive model using the same parameters as those in Fig. 3. As shown in Fig. 4, the additional resistance affects the PCAR spectra in the purely diffusive regime in a manner similar to that in the purely ballistic regime. Indeed, since the additional resistance originates from the pseudo-four-probe method of the point-contact experiment, our analysis should be independent of theoretical models and applicable for all PCAR analysis.

VIII. SELF-CONSISTENT METHOD FOR EXTRACTING dI_{NS}/dV_{AR} FROM THE MEASURED dI_{NS}/dV

In the calculated PCAR spectra in Figs. 3 and 4, the voltage V_{AR} is used as a known parameter to calculate the total differential conductance dI_{NS}/dV and the total voltage V .

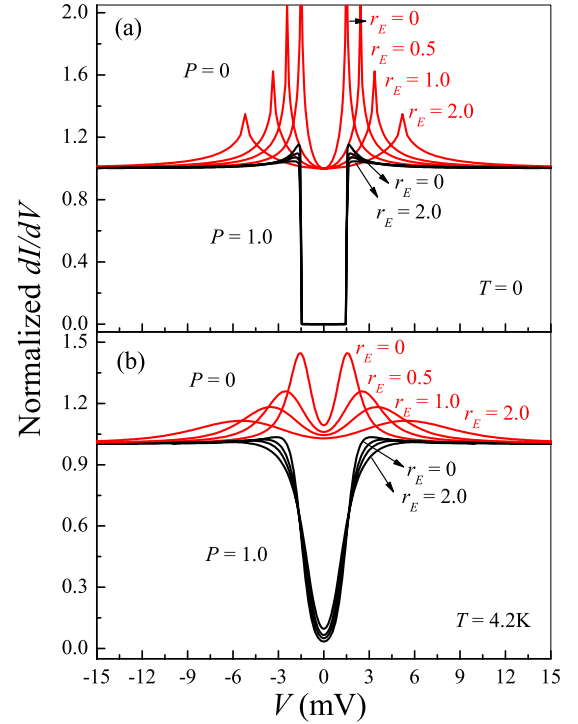


FIG. 4. (Color online) Calculated PCAR spectra in the purely diffusive regime with various $r_E=0, 0.5, 1.0, 2.0$ for $P=0$ and 1.0 at (a) $T=0$ and (b) $T=4.2$ K.

However, in an actual experiment one measures dI_{NS}/dV as a function of V without knowing V_{AR} a priori. To carry out the data analysis, V_{AR} must be determined first so that the experimental data can be compared with theoretical models to extract the parameters such as P, Z , and Δ . At first glance, it appears that V_{AR} can be easily obtained from V through $V_{AR} = VR_{AR}/(R_{AR} + R_E)$. However, because R_{AR} depends on V_{AR} due to the AR process, the contact voltage V_{AR} cannot be determined analytically. We use a self-consistent method to numerically determine V_{AR} from V . Initially, we first set $V_{AR} = V$, then calculate I_{NS} from V_{AR} and obtain $R_{AR} = V_{AR}/I_{NS}$ and a new contact voltage $V'_{AR} = VR_{AR}/(R_{AR} + R_E)$. We repeat the iterative procedure self-consistently until V'_{AR} is indistinguishable from V_{AR} , we then calculate dI_{NS}/dV from the determined V_{AR} .

Next we verify our self-consistent method by comparing the calculated data (dI_{NS}/dV vs V) with the accurately generated data using V_{AR} as a known parameter. As shown in Fig. 5(a), the solid line is the best fit using the self-consistent method while the open circles are the data generated using the parameters listed in the up left-hand corner of Fig. 5(a). The best-fit parameters (upper right-hand corner) obtained by the method are precisely those of the original parameters used for calculating the data. Even when substantial random noises have been manually added to the generated data as shown in Fig. 5(b) (open circles), the best-fit parameters obtained using our method are still very close to the original parameters, as listed in the upper right-hand corner of Fig. 5(b). This further validates our self-consistent method.

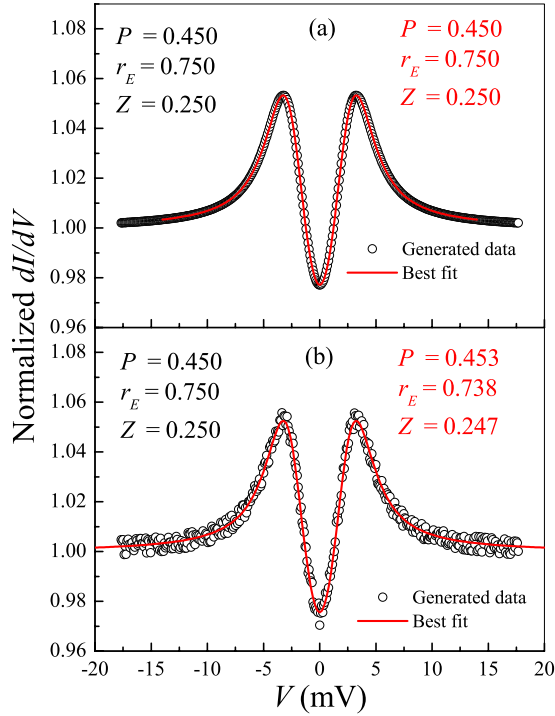


FIG. 5. (Color online) Generated dI/dV as a function of V (open circles) using V_{AR} (see text) as a known variable and other parameter list on the left corner, and the best fit (solid line) to the generated data using the self-consistent method and resultant parameters listed on the right corner: (a) without and (b) with a randomly generated noise added.

IX. ANALYSES OF PCAR SPECTRA ON THIN FILMS WITH HIGH RESISTIVITY

We have discussed the effect of the unavoidable additional resistance due to the pseudo-four-probe method of the point-contact geometry and demonstrated that it can radically alter the PCAR spectra. We have also demonstrated a self-consistent method to calculate the true differential conductance. Next, we apply our method to investigate some actual experimental PCAR spectra. As discussed above, because the effect of the additional resistance is more observable in diffusive contacts, we use Nb tip in contact with an amorphous ferromagnetic CoFeB thin film with a high resistivity of $167 \mu\Omega \text{ cm}$. We also investigate the effect of the sample resistivity on the additional resistance by annealing the same sample to acquire a smaller resistivity of $19 \mu\Omega \text{ cm}$.

The Nb tip we used has been made from a $0.030''$ wire with a resistivity ratio of $\rho(300 \text{ K})/\rho(10 \text{ K})=49.4$ and superconducting transition temperature of 9.27 K as measured by a four-probe method. The superconducting gap of the Nb tip is $0.97 \times 1.83k_B T_C = 1.42 \text{ meV}$ at 4.2 K , where the coefficient 1.83 , slightly larger than the BCS value of 1.764 ,³³ has been used by previous work³⁴ and 0.97 is a factor due to the finite temperature effect. The $\text{Co}_{40}\text{Fe}_{40}\text{B}_{20}$ (CFB) thin film has been made by magnetron sputtering from a composite target. The resistivity of as-deposited sample is $167 \mu\Omega \text{ cm}$ at 5 K and it is reduced to $19 \mu\Omega \text{ cm}$ after crystallization by annealing at high temperatures.²¹

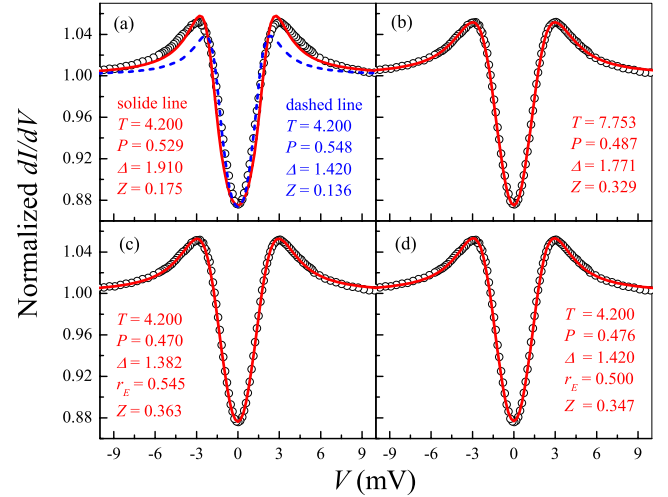


FIG. 6. (Color online) Analyses of one representative PCAR spectrum (open circles) from a Nb-CoFeB point contact. Best fit using the ballistic model [(a) and (b)] without and [(c) and (d)] with the inclusion of r_E . (a) Solid line (varying P , Δ , and Z) and dashed line (varying P and Z). (b) Solid line (varying T , P , Δ , and Z varied). (c) Solid line (varying T , P , Δ , r_E , and Z with $T=4.2 \text{ K}$) and (d) Solid line (varying P , r_E , and Z with $T=4.2 \text{ K}$ and $\Delta=1.42 \text{ meV}$).

One representative PCAR spectrum of Nb-CFB contact taken at 4.2 K has been analyzed with different procedures using the ballistic model as shown in Fig. 6. When T has been fixed at the experimental temperature of 4.2 K and varying parameters P , Δ , and Z , but without taking the additional resistance R_E into account, the best-fit curve deviates significantly from the data especially near the two peaks, as shown in Fig. 6(a) (solid line). Also disturbingly, the resultant gap value Δ is 1.91 meV , much larger than the expected value of 1.42 meV . However, if both Δ and T have been fixed to the experimental values 1.42 meV and 4.2 K , the fit is clearly unsatisfactory; falling far off the data as shown by the dashed line in Fig. 6(a). If we allowed temperature T as well as P , Δ , and Z as fitting parameters, the best-fit curve follows the data quite well as shown in Fig. 6(b). But the resultant $T=7.75 \text{ K}$ is much higher than the experimental temperature of 4.2 K and the gap is 1.77 meV , also much larger than the gap value of 1.42 meV for Nb. These are the high effective temperature and gap anomalies encountered by others as well.²⁹

In the new formalism, when R_E has been properly taken into account, the data can be described by the best-fit parameters very well when T and Δ are fixed as experimental values as shown in Fig. 6(d). The determined P value is 0.476 , smaller than the values from 0.487 to 0.548 as in Figs. 6(a) and 6(b). Even when only $T=4.2 \text{ K}$ is fixed and allowing other parameters to vary as shown in Fig. 6(c), the best-fit parameters are still very close to those in Fig. 6(d) where T and Δ have been fixed to the experimental values.

We have made over 100 contacts on the as-deposited amorphous CFB films and over 50 contacts on the annealed crystallized CFB films using the Nb tips. For different contacts, the additional resistance is different because of the variation in position and geometry of the contact. It is of

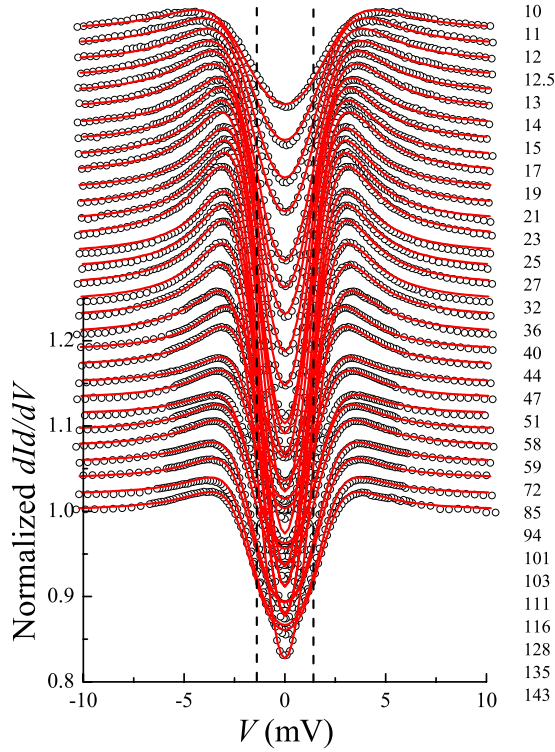


FIG. 7. (Color online) A series of PCAR spectra (open circles) of Nb-CoFeB contacts with various contact resistances (listed on the right) achieved by gradually pressing the tip, with solid lines the best fit to the experimental data and parameters listed in Fig. 8. The two vertical lines indicate $\pm\Delta/e = \pm 1.42$ mV, the gap value for Nb at 4.2 K.

interest to study one series of contacts where the geometrical factors remain the same and only the contact resistance varies. Figure 7 shows one of such series of contacts with resistance varying from 143 to 10 Ω , achieved by gradually pressing the tip after each measurement. The open circles are the experimental data and the solid lines are the best-fit results using the ballistic model with the additional resistance taken into account. First of all, all the data can be well described by our model. During the analysis, the experimental values $T=4.2$ K and $\Delta=1.42$ meV have been used. One notes the locations of the two AR peaks remain essentially the same for total resistance $R > 15 \Omega$ spectra but visibly different (broader and shifting to higher voltage) for those at $R < 15 \Omega$, indicating the effect of R_E for those larger contacts.

The best-fit parameters of the spectra shown in Fig. 7 for Nb on the as-deposited amorphous CFB films are shown as squares in Fig. 8. As the R increases from 9 to 15 Ω , the relative extra resistance r_E decreases rapidly from 1.1 to about 0.5 and remains at about 0.5 for R values from 15 to 143 Ω as shown in Fig. 8(a). From the definition of $r_E = R_E/R_{NN} = R_E/(R - R_E)$, if the additional resistance R_E is the sample resistance R_S between the point contact and the voltage lead, then in these series of measurements with fixed electrodes, R_S and R_E should not vary and be independent of R . In this case, the value of r_E should diverge at $R = R_E$ and approach zero at large R . In our experiment, as shown in Fig.

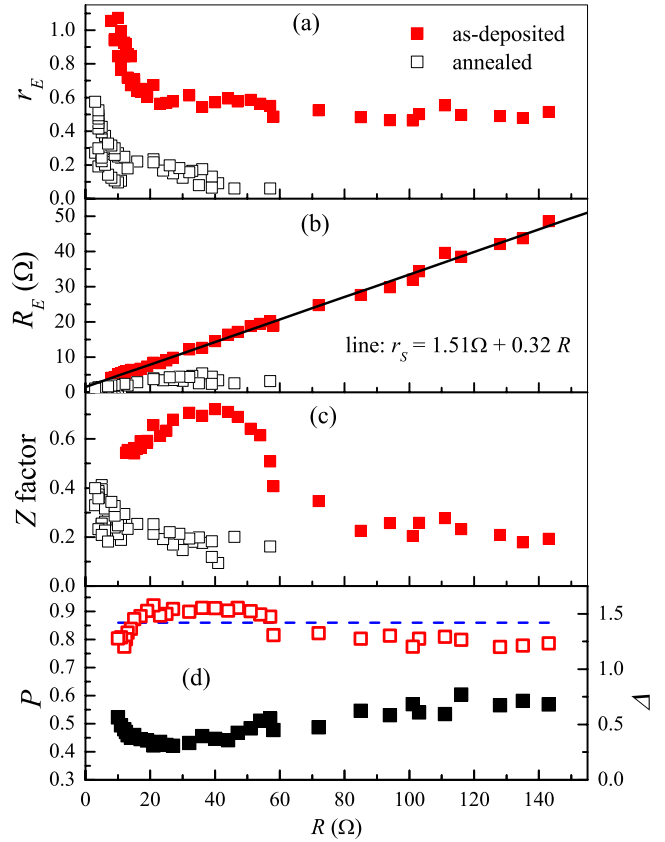


FIG. 8. (Color online) Parameters of the best fits shown in Fig. 7: (a) the relative additional resistance r_E , (b) the additional resistance R_E , (c) the Z factor, and (d) the spin polarization P (solid squares) using the left scale, as a function of the total resistance R . Also shown in (d) are the values of the superconducting gap Δ (open squares) using the right scale obtained with varying P , r_E , Δ , and Z with T fixed at 4.2 K. The horizontal dashed line shows the value of 1.42 meV of Nb.

8(a), the value of r_E appears to diverge at $R \approx 9 \Omega$ and approaches a constant value of about 0.5 instead of zero for $R > 15 \Omega$. The resistance between the point contact and the voltage lead on the film is only 1.5 Ω , which has been measured experimentally and it is consistent with the calculation from the resistivity and the dimensions of the sample. The value of $R_E = 9 \Omega$ is much larger than the value of 1.5 Ω .

The apparent discrepancy between $R_E = 9 \Omega$ and the measured sample resistance of 1.5 Ω is due to the incorrect notion that the additional resistance is mostly from the sample resistance and independent of the contact resistance. Fortunately, the absolute value of the extra resistance R_E can be calculated for each contact from R and r_E using $R_E = r_E R / (1 + r_E)$, which is plotted in Fig. 8(b) (solid square). As vividly displayed, R_E is not a constant at all. The value of R_E increases quasilinearly with R from less than 5 Ω at $R = 9 \Omega$ to as large as 50 Ω at $R = 143 \Omega$. This linear dependence is due to the fact that from $R = 15$ to $R = 143 \Omega$, $r_E \approx 0.5$ as shown in Fig. 8(a). Therefore in this range of R , $R_E = r_E R / (1 + r_E) \approx 0.32R$. More accurate analyses show that $R_E = 1.51 \Omega + 0.32R$, where the constant value of 1.51 Ω is the resistance between the contact and the fixed voltage lead. In these experiments, it is clearly revealed that even with

fixed leads R_E increases with R . It is erroneous to assume that the additional resistance would be the same because the measuring geometry and the voltage lead remain unchanged. We recall that $R=R_C+R_S=R_{AR}+R_E$ and that $R_S=1.51\ \Omega$. One can find the contact resistance and the Andreev resistance for each of these Nb-CFB contacts as $R_C=R-R_S=R-1.51\ \Omega$ and $R_{AR}=R-R_E=0.68R-1.51\ \Omega$. The determined P value as a function of R is shown in Fig. 8(d) (solid squares) with the left scale. Similar to other PCAR studies, the P value depends on the Z factor and varying from about 0.6 at $Z=0.1-0.4$ at $Z=0.8$, consistent with previous reports.²¹ The intrinsic P value can be obtained by extrapolating Z to zero, although with caution for materials with very large mismatch in Fermi velocity.^{15,16}

In the above discussion, both the superconducting gap Δ and the temperature T have been fixed at the experimental values. In addition to the determination of spin polarization, PCAR is also a powerful tool to measure the superconducting gap of a superconductor, which is not known *a priori*. We repeated the analysis with only T fixed at the experimental temperature, and allowing P , r_E , Z , and Δ to vary, as demonstrated in Fig. 6(c). The best-fit results of all the parameters are within 10% of those with Δ fixed at 1.42 meV. Equally important, the determined gap value, using the right scale in Fig. 8(d), is very close to the dashed line, the value of $\Delta=1.42$ meV expected from Nb. It should be noted that the values of $\Delta=\pm 1.42$ meV are shown as the vertical lines in Fig. 7. Because of the pronounced effects of the additional resistance, all the PCAR spectra in Fig. 7 show apparent gap *much larger* than $\Delta=1.42$ meV, indeed more than 2Δ , and yet our analyses correctly show that the superconducting gap remains essentially unchanged at $\Delta=1.42$ meV. These analyses demonstrate clearly that with the additional resistance appropriately taken into account in our method, we can reliably extract the correct P value, as well as the Δ value.

Essential to our analyses is $R=R_{AR}+R_E$, the separation of the Andreev resistance R_{AR} and the additional resistance R_E . We comment on the important physical meaning of the Andreev resistance R_{AR} . Ideally, the AR process occurs only at the point-contact interface. In reality, electrons in the vicinity of the interface are compelled by the bias voltage to participate in the AR process. This AR region should be related to size of the mean-free path or the spin-diffusion length of the material in contact thus is an intrinsic property of the material. The ratio R_{AR}/R_C indicates the portion of the contact resistance involved in the AR process. For these Nb-CFB contacts, $R_{AR}/R_C=(0.68R-1.51)/(R-1.51)\approx 0.68$ is a constant since $R\gg 1.51\ \Omega$, showing only 68% of the contact resistance is involved in the AR process for all of these contacts. The large resistivity of $167\ \mu\Omega\text{ cm}$ in the as-deposited film indicates all these contacts are close to the purely diffusive limit. An estimation using the Maxwell resistance formula shows that the AR process occurs effectively only in a region of $1.82a$, less than the contact diameter $2a$ for all of these contacts.

X. ANALYSES OF PCAR SPECTRA ON THIN FILMS WITH MEDIUM RESISTIVITY

We have also experimentally investigated the effects of the additional resistance in point contacts on materials with a

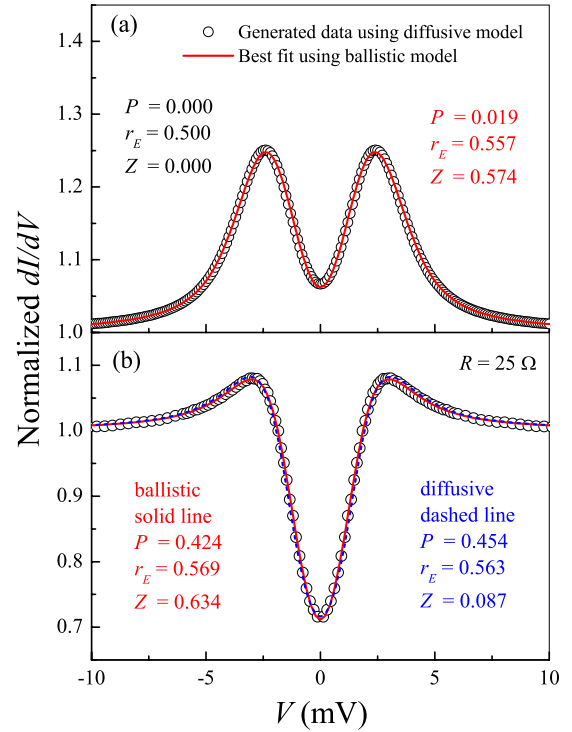


FIG. 9. (Color online) (a) Best fit using the ballistic model to the data generated by the diffusive model and (b) best fit to one experimental PCAR spectrum data with $R=25\ \Omega$ using both ballistic and diffusive models with the inclusion of the additional resistance, with the respective parameters listed in the panel.

lesser resistivity. While the resistivity of the as-prepared amorphous CFB film is about $167\ \mu\Omega\text{ cm}$, the resistivity of the crystallized CFB film is only about $19\ \mu\Omega\text{ cm}$ after annealing at 450° for 12 h in vacuum. The PCAR spectra (not shown) of Nb in contact with annealed CFB can again be well described by the ballistic model with the inclusion of the additional resistance. The extracted parameters are shown in Fig. 8 as open squares with the experimental conditions of $T=4.25\ \text{K}$ and $\Delta=1.42\ \text{meV}$. As shown in Fig. 8, r_E , R_E , and Z factor are much smaller than those in contacts on the as-deposited samples with higher resistivity, revealing the pronounced effects of high resistivity. This is because the point contacts on materials with a smaller resistivity, hence a larger mean-free path, are closer to the purely ballistic region. As discussed above, the value of R_E in ballistic contacts is much smaller than that in diffusive contacts. At about $R=5\ \Omega$, r_E rapidly increases to about 0.6. The absolute value of the extra resistance R_E for each contact, calculated from R and r_E , is shown in Fig. 8(b). The value R_E (open squares) behaves differently from those of contacts with the as-deposited sample (solid squares). At large R , R_E is small and increasing slightly as R decrease. It decreases when R is less than about $30\ \Omega$ and at very small R ($<10\ \Omega$) it nearly follows a linear dependence as that in contacts with the as-deposited samples but with an obviously smaller slope. This is because at very small R in which the contact size are very large, the contacts are close to the diffusive region, thus obeying the linear dependence as in the case of contacts on the as-deposited sample with large resistivity.

XI. BALLISTIC VS DIFFUSIVE CONTACTS

Theoretically, a point contact can be treated in two extreme regimes: purely ballistic and purely diffusive. Experimentally, however, an actual point contact is neither purely ballistic nor purely diffusive but rather between the two extreme cases. Fortunately, it has been shown that the purely ballistic model can be used to analyze the results in the purely diffusive regime, arriving with essentially the same parameters except the Z factor.²⁷ Therefore, the ballistic model can be used to analyze the PCAR spectra of any point contacts, including those of diffusive nature. All the parameters extracted from the PCAR spectra remain valid except that of the Z factor.

With the inclusion of the additional resistance R_E , as discussed above, R_E affects the PCAR spectra similarly for both the ballistic and the diffusive models. It is also important to ascertain whether the ballistic model can still describe the results in the diffusive regime. We first use the ballistic model¹⁸ to analyze the PCAR spectrum calculated from the diffusive model with parameters $P=0.0$, $r_E=0.5$, and $Z=0.0$. As shown in Fig. 9(a), the data from the diffusive model can be well described by the ballistic model with similar P and r_E values, except the Z factor of 0.57. This demonstrates that with our analysis, regardless of diffusive or ballistic contacts, similar P value and r_E values can still be reliably obtained except the Z factor. We then subject the actual PCAR spectrum from Fig. 7 with $R=25 \Omega$ to both models including r_E , as shown in Fig. 9(b). The spectrum can again be well described by both models and the best-fit parameters P and r_E are very similar to each other except the Z factor. This demonstrates that when the additional resistance has been correctly taken into account, the purely ballistic model can be reliably used to analyze the PCAR spectra to obtain the spin polarization, the superconducting gap, and the values of R_{AR} ,

R_E , R_S , and R_C for both ballistic and diffusive contacts, except the Z factor, which describes the imperfection of the contact and not of physical significance.

XII. SUMMARY

In summary, we have shown that in PCAR experiments the additional resistance due to the pseudo-four-probe electrical measurements of point contacts, either diffusive or ballistic, can greatly affect the PCAR spectra, particularly in contacts with materials with large resistivity. There are two contributions to the additional resistance: the Andreev resistance R_{AR} , which is involved in the Andreev reflection process, and the additional resistance R_E , which is not. We show a detailed theoretical analysis with the additional resistance taken into account. Equally important, it is essential to perform a self-consistent analysis of the experimental conductance dI_{NS}/dV to extract the intrinsic Andreev conductance dI_{NS}/dV_{AR} , which is the conductance that can be correctly normalized. Experimentally, using contacts on materials with very different resistivity, we have demonstrated the applicability of our analytical process and determined the additional resistance. We also show this new method can be applied to all contacts, ballistic as well as diffusive. The information of all the physically important quantities, the superconducting gap of the superconductor, spin polarization of the metal, and the temperature of the measurement, can be reliably obtained. We have addressed the critical issue of the additional resistance, and significantly advanced the point-contact Andreev reflection spectroscopy, a key technique for quantitatively measuring spin polarization and superconducting gap.

ACKNOWLEDGMENT

Work supported by the National Science Foundation.

*Present address: Department of Physics, Arizona State University, Tempe, Arizona 85287-1504

¹S. A. Wolf, D. D. Awschalom, R. A. Buhrman, J. M. Daughton, S. von Molnar, M. L. Roukes, A. Y. Chitchekanova, and D. M. Treger, *Science* **294**, 1488 (2001).

²I. Žutić, J. Fabian, and S. Das Sarma, *Rev. Mod. Phys.* **76**, 323 (2004).

³R. Meservey and P. M. Tedrow, *Phys. Rep.* **238**, 173 (1994).

⁴J. S. Moodera and G. Mathon, *J. Magn. Magn. Mater.* **200**, 248 (1999).

⁵D. J. Monsma and S. S. P. Parkin, *Appl. Phys. Lett.* **77**, 720 (2000).

⁶S. S. P. Parkin, C. Kaiser, A. Panchula, P. M. Rice, B. Hughes, M. Samant, and S. Yang, *Nature Mater.* **3**, 862 (2004).

⁷J. M. D. Teresa, A. Barthelémy, A. Fert, J. P. Contour, and F. M., P. Seneor, *Science* **286**, 507 (1999).

⁸R. L. Long, V. W. Hughes, J. S. Greenberg, I. Ames, and R. L. Christensen, *Phys. Rev.* **138**, A1630 (1965).

⁹E. Kisker, W. Gudat, E. Kuhlmann, R. Clauberg, and M. Campagna, *Phys. Rev. Lett.* **45**, 2053 (1980).

¹⁰C. Rau, K. Waters, and N. Chen, *Phys. Rev. Lett.* **64**, 1441 (1990).

¹¹A. F. Andreev, *Zh. Eksp. Teor. Fiz.* **46**, 1823 (1964) [*Sov. Phys. JETP* **19**, 1228 (1964)].

¹²T. Y. Chen, Z. Tesanovic, R. H. Liu, X. H. Chen, and C. L. Chien, *Nature (London)* **453**, 1224 (2008).

¹³S. K. Upadhyay, A. Palanisami, R. N. Louie, and R. A. Buhrman, *Phys. Rev. Lett.* **81**, 3247 (1998).

¹⁴R. J. Soulen, Jr., J. M. Byers, M. S. Osofsky, B. Nadgorny, T. Ambrose, S. F. Cheng, P. R. Broussard, C. T. Tanaka, J. Nowak, J. S. Moodera, A. Barry, and J. M. D. Coey, *Science* **282**, 85 (1998).

¹⁵I. Žutić and S. Das Sarma, *Phys. Rev. B* **60**, R16322 (1999).

¹⁶I. Žutić and O. T. Valls *Phys. Rev. B* **61**, 1555 (2000).

¹⁷G. J. Strijkers, Y. Ji, F. Y. Yang, C. L. Chien, and J. M. Byers, *Phys. Rev. B* **63**, 104510 (2001).

¹⁸I. I. Mazin, A. A. Golubov, and B. Nadgorny, *J. Appl. Phys.* **89**, 7576 (2001).

¹⁹P. Chalsani, S. K. Upadhyay, O. Ozatay, and R. A. Buhrman, *Phys. Rev. B* **75**, 094417 (2007).

- ²⁰T. Y. Chen, C. L. Chien, and C. Petrovic, *Appl. Phys. Lett.* **91**, 142505 (2007).
- ²¹S. X. Huang, T. Y. Chen, and C. L. Chien, *Appl. Phys. Lett.* **92**, 242509 (2008).
- ²²B. Nadgorny, I. I. Mazin, M. Osofsky, R. J. Soulen, Jr., P. Brousard, R. M. Stroud, D. J. Singh, V. G. Harris, A. Arsenov, and Y. Mukovskii, *Phys. Rev. B* **63**, 184433 (2001).
- ²³Y. Ji, C. L. Chien, Y. Tomioka, and Y. Tokura, *Phys. Rev. B* **66**, 012410 (2002).
- ²⁴L. Wang, K. Umemoto, R. M. Wentzcovitch, T. Y. Chen, C. L. Chien, J. G. Checkelsky, J. C. Eckert, E. D. Dahlberg, and C. Leighton, *Phys. Rev. Lett.* **94**, 056602 (2005).
- ²⁵Y. Ji, G. J. Strijkers, F. Y. Yang, C. L. Chien, J. M. Byers, A. Anguelouch, G. Xiao, and A. Gupta, *Phys. Rev. Lett.* **86**, 5585 (2001).
- ²⁶J. S. Parker, S. M. Watts, P. G. Ivanov, and P. Xiong, *Phys. Rev. Lett.* **88**, 196601 (2002).
- ²⁷G. T. Woods, R. J. Soulen, Jr., I. I. Mazin, B. Nadgorny, M. S. Osofsky, J. Sanders, H. Srikanth, W. F. Egelhoff, and R. Datla, *Phys. Rev. B* **70**, 054416 (2004).
- ²⁸T. W. Chiang, Y. H. Chiu, S. Y. Huang, S. F. Lee, J. J. Liang, H. Jaffrès, J. M. George, and A. Lemaitre, *J. Appl. Phys.* **105**, 07C507 (2009).
- ²⁹N. Auth, G. Jakob, T. Block, and C. Felser, *Phys. Rev. B* **68**, 024403 (2003).
- ³⁰R. S. Timsit, in *Electrical Contacts: Principles and Applications*, edited by P. G. Slade (Marcel Dekker, New York, 1999), Chap. 1.
- ³¹Yu. V. Sharvin, *Zh. Eksp. Teor. Fiz.* **48**, 984 (1965) [*Sov. Phys. JETP* **21**, 655 (1965)].
- ³²G. E. Blonder, M. Tinkham, and T. M. Klapwijk, *Phys. Rev. B* **25**, 4515 (1982).
- ³³M. Tinkham, *Introduction to Superconductivity*, 2nd ed. (McGraw-Hill, New York, 1996), p. 9.
- ³⁴D. K. Finnemore, T. F. Stromberg, and C. A. Swenson, *Phys. Rev.* **149**, 231 (1966).